

This is a repository copy of *Variation of terpene alkaloids in Daphniphyllum macropodum across plants and tissues*.

White Rose Research Online URL for this paper:

<https://eprints.whiterose.ac.uk/id/eprint/212767/>

Version: Published Version

---

**Article:**

Eljounaidi, Kaouthar orcid.org/0000-0003-4675-226X, Radzikowska, Barbara A, Whitehead, Caragh B et al. (10 more authors) (2024) Variation of terpene alkaloids in *Daphniphyllum macropodum* across plants and tissues. *The New phytologist*. pp. 299-313. ISSN: 1469-8137

<https://doi.org/10.1111/nph.19814>

---

**Reuse**










This article is distributed under the terms of the Creative Commons Attribution (CC BY) licence. This licence allows you to distribute, remix, tweak, and build upon the work, even commercially, as long as you credit the authors for the original work. More information and the full terms of the licence here:

<https://creativecommons.org/licenses/>

**Takedown**

If you consider content in White Rose Research Online to be in breach of UK law, please notify us by emailing [eprints@whiterose.ac.uk](mailto:eprints@whiterose.ac.uk) including the URL of the record and the reason for the withdrawal request.

# Variation of terpene alkaloids in *Daphniphyllum macropodum* across plants and tissues

Kaouthar Eljounaidi<sup>1</sup> , Barbara A. Radzikowska<sup>1,2</sup> , Caragh B. Whitehead<sup>1</sup>, Danielle J. Taylor<sup>1</sup>, Susana Conde<sup>3</sup>, William Davis<sup>1</sup> , Adam A. Dowle<sup>4</sup> , Swen Langer<sup>4</sup> , Sally James<sup>4</sup> , William P. Unsworth<sup>2</sup> , Daphne Ezer<sup>3</sup> , Tony R. Larson<sup>4</sup>  and Benjamin R. Lichman<sup>1</sup> 

<sup>1</sup>Centre for Novel Agricultural Products, Department of Biology, University of York, York, YO10 5DD, UK; <sup>2</sup>Department of Chemistry, University of York, York, YO10 5DD, UK;

<sup>3</sup>Department of Biology, University of York, York, YO10 5DD, UK; <sup>4</sup>Biosciences Technology Facility, Department of Biology, University of York, York, YO10 5DD, UK

## Summary

Author for correspondence:  
Benjamin R. Lichman  
Email: [benjamin.lichman@york.ac.uk](mailto:benjamin.lichman@york.ac.uk)

Received: 8 February 2024  
Accepted: 28 April 2024

New Phytologist (2024)  
doi: 10.1111/nph.19814

**Key words:** alkaloids, biosynthesis, *Daphniphyllum*, metabolomics, specialised metabolism.

- *Daphniphyllum macropodum* produces alkaloids that are structurally complex with polycyclic, stereochemically rich carbon skeletons. Understanding how these compounds are formed by the plant may enable exploration of their biological function and bioactivities.
- We employed multiple metabolomics techniques, including a workflow to annotate compounds in the absence of standards, to compare alkaloid content across plants and tissues.
- Different alkaloid structural types were found to have distinct distributions between genotypes, between tissues and within tissues. Alkaloid structural types also showed different isotope labelling enrichments that matched their biosynthetic relationships.
- The work suggests that mevalonate derived 30-carbon alkaloids are formed in the phloem region before their conversion to 22-carbon alkaloids which accumulate in the epidermis. This sets the stage for further investigation into the biosynthetic pathway.

## Introduction

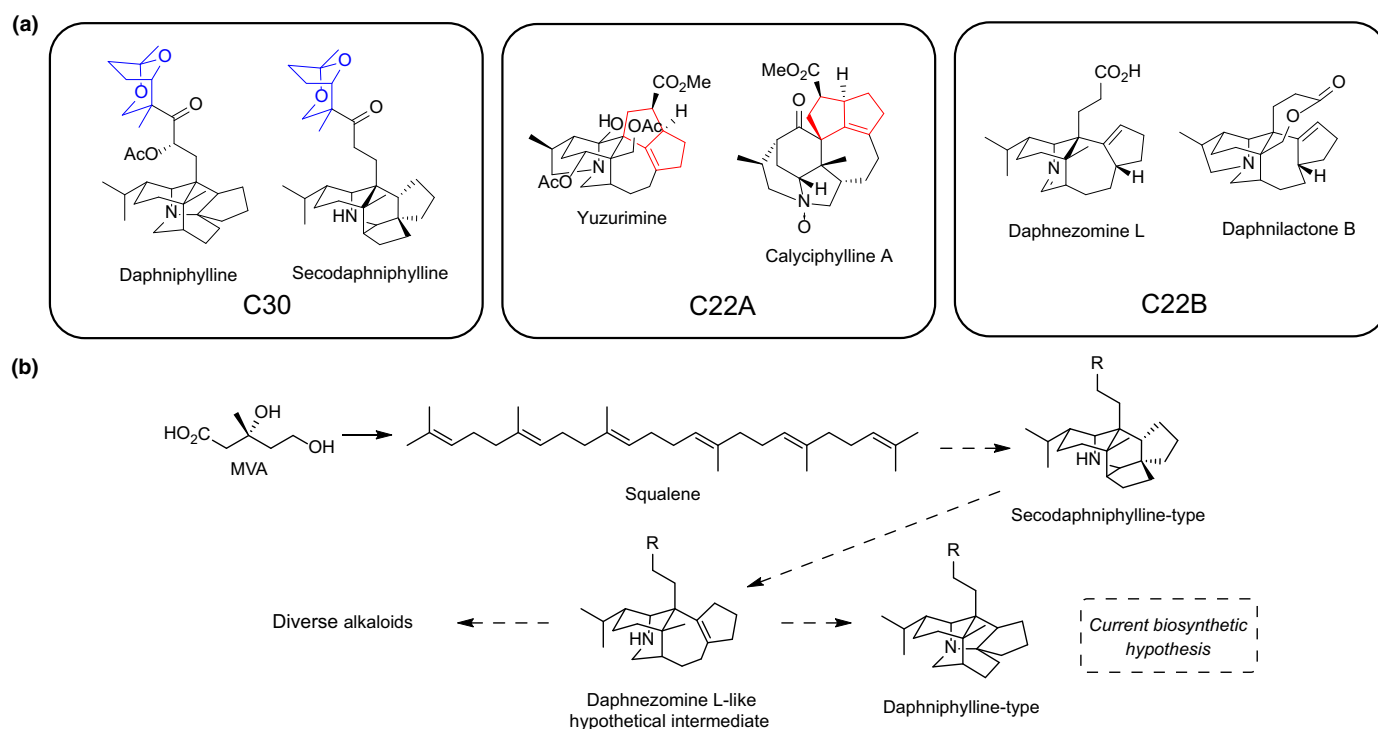
Plants biosynthesise a plethora of specialised metabolites which have various roles including providing defence against herbivores, protection against abiotic stress, and mediation of interspecies communication (Mithöfer & Boland, 2012; Erb & Kliebenstein, 2020). Alkaloids are nitrogen-containing natural products typically with amino acid origins (Lichman, 2021), many of which have acute biological activities, for example acting as toxins or behavioural modulators (Pluskal & Weng, 2018). Alkaloids are extensively used by humans as therapeutics and analgesics, and their natural diversity remains a source of novel pharmaceuticals (Bharate *et al.*, 2018).

Plants from *Daphniphyllum* (Family: Daphniphyllaceae, Order: Saxifragales) are dioecious shrubs or small trees native to tropical and subtropical Asia. These evergreens are often grown as ornamental plants due to their characteristic red petioles and dark green leaves (Boyce, 1999). Some *Daphniphyllum* species have also been used in traditional Chinese medicines to treat asthma, rheumatism, and snake-bites (Wu *et al.*, 2013). *Daphniphyllum* sp. are known for their ability to produce structurally diverse and complex alkaloids characterised by polycyclic cage-like structures and stereochemically rich molecular frameworks (Fig. 1a) (Chattopadhyay & Hanessian, 2017).

More than 330 *Daphniphyllum* alkaloids (DA) have been identified to date. Based on their skeletal structures, DAs can be categorised into up to *c.* 35 structurally unique subtypes including daphniphylline, secodaphniphylline, calyciphylline A and yuzurimine subtypes (Guo *et al.*, 2020a). At a higher level, DAs can also be classified by the number of carbons in their core skeleton: C30 or C22, and the latter group can also further be classified by the presence (C22A) or absence (C22B) of a hexahydropentalene moiety (two fused five membered rings) (Fig. 1a).

*Daphniphyllum* alkaloids may be involved in plant defence in a similar manner to other alkaloids (Wink, 2015; Chowański *et al.*, 2016). This is supported experimentally by the observation of insecticidal bioactivities reported for a small number of compounds (Li *et al.*, 2009). Human related DA bioactivities include anti-inflammatory (Yang *et al.*, 2021), neuroprotective (Saito *et al.*, 2008) and anti-cancer effects (Zhang *et al.*, 2009; He *et al.*, 2011; Cao *et al.*, 2013). Due to their structural complexity and potential biological activities, DAs have remained targets for total synthesis efforts over many decades (Heathcock *et al.*, 1986; Pietre & Heathcock, 1990; Heathcock & Stafford, 1992; Weiss & Carreira, 2011; Guo *et al.*, 2019, 2020b).

First insights into the biosynthesis of DAs was from isotope feeding studies. Feeding *D. macropodium* aerial tissues with labelled mevalonic acid (MVA) led to isolation of daphniphylline



**Fig. 1** *Daphniphyllum* alkaloids. (a) Representative *Daphniphyllum* alkaloids, classified by carbon skeleton (C30 vs C22, blue highlighting C8 fragment lost in C22 compounds) and presence (C22A) or absence (C22B) of hexahydropentalene ring (red). (b) Proposed pathway via squalene and a secodaphniphylline type precursor into diverse alkaloids subtypes.

and codaphniphylline alkaloids (C30) labelled with six MVA units (Suzuki *et al.*, 1973). A similar experiment conducted in *D. teijsmannii* fruit led four MVA units incorporation into daphnilactone B (C22) (Niwa *et al.*, 1973). In *D. macropodium*, incorporation of squalene showed DAs to be triterpene in origin (Suzuki *et al.*, 1973). The majority of reported triterpene alkaloids are steroidal alkaloids such as solanine from Solanaceae and cyclopamine from *Veratrum californicum* (Cherney & Baran, 2011; Itkin *et al.*, 2013; Augustin *et al.*, 2015); however, DAs do not appear to be steroidal in origin.

Pioneering biomimetic syntheses by Heathcock demonstrated formation of a secodaphniphylline skeleton from a linear oxidised squalene (Fig. 1b) (Pietre & Heathcock, 1990; Heathcock, 1996). The daphniphylline skeletons can be formed via biomimetic conversions from secodaphniphylline type (Heathcock & Joe, 1995) or daphnilactone B-like compounds (Niwa *et al.*, 1974). These experiments, alongside chemical logic, indicate that secodaphniphylline is a universal precursor, which can be converted into a reactive intermediate, which in turn is a branch point to diverse DAs (Fig. 1b) (Morita & Kobayashi, 2007). The formation of the hexahydropentalene ring of the C22A DAs is relatively late in the pathway (Fig. 1b) (Mu *et al.*, 2008; Kobayashi & Kubota, 2009).

The biosynthesis of complex alkaloids in plants often has a spatial element, with different steps of the pathway occurring in different tissues or cell types, with transportation of pathway intermediates between these locations (Bird *et al.*, 2003;

Mahroug *et al.*, 2007). For example, pyrrolizidine alkaloids from *Senecio vulgaris* are translocated via the phloem from roots to aerial organs (Ehmke *et al.*, 1988; Witte *et al.*, 1990). In *Catharanthus roseus*, different steps of alkaloid biosynthesis are localised to specific cell types in the leaf (Yamamoto *et al.*, 2016, 2019; Li *et al.*, 2023). In *Daphniphyllum* spp., there have been reports of different alkaloids being isolated from different regions of the plant (Mu *et al.*, 2008; Shuzhen *et al.*, 2013), but no systematic assessment into the spatial distribution of the alkaloids has been conducted. Elucidation of the biosynthetic origins of the alkaloids, as well as understanding their biological function, is dependent on knowledge of their distribution within the plant.

To map alkaloid distribution in *D. macropodium* we combined high-resolution liquid chromatography tandem mass spectrometry (HR-LC-MS/MS), isotope feeding and mass spectral imaging. We observed alkaloid structural types differentially distributed across plants, tissues, and cell types. Overall, we determined that 30-carbon alkaloids, formed from six isoprene units, accumulate in the phloem before their conversion to 22-carbon alkaloids (and loss of two isoprene units). The C22 alkaloids, especially those with a hexahydropentalene moiety (i.e. C22A such as yuzurimine) accumulate in the epidermis and were enriched in immature leaves. This study sets the stage for future work on *Daphniphyllum* alkaloid biosynthesis and highlights how integrating different metabolomics strategies can reveal valuable insights on compound distribution within the plant.

## Materials and Methods

### Chemical database and standards

An *in silico* *Daphniphyllum* Blume natural product database was manually assembled from Reaxys (<https://www.reaxys.com/>, Elsevier; query: for substances ‘Isolated from Natural Source: *Daphniphyllum*’) and recent reviews and research articles (Kobayashi & Kubota, 2009; Chattopadhyay & Hanesian, 2017). Each *Daphniphyllum* alkaloid (DA) was assigned to a structural subtype using definitions from Chattopadhyay & Hanesian (2017). *Daphniphylline* and *yuzurimine* standards were obtained from plant tissue and verified by NMR (Supporting Information Methods S1). Other standards were purchased from commercial vendors (Table S1).

### Hydroponic growth

*Daphniphyllum macropodum* Miq. seeds were harvested when the fruit was ripe (dark purple/blue). The fleshy tissue (epicarp and mesocarp) was removed, and the seed rinsed with water and air-dried. The seed was sterilised with chlorine vapor for 5 h and then transferred to Petri dishes containing seed germination media (gelrite (0.5% w/v), Lloyd and McCown’s woody plant medium with vitamins (50% strength), Plant Preservative Mixture (1 ml l<sup>-1</sup>), streptomycin (50 µg ml<sup>-1</sup>), cefotaxime (250 µg ml<sup>-1</sup>), gibberellic acid 4 + 7 (200 µg ml<sup>-1</sup>), pH 5.8). The seeds were incubated (14 h : 10 h, 20°C : 10°C; dark) until radicle emergence, when they were placed in stratification conditions (4°C). After 14 d, incubation conditions were modified and light introduced (1 h, 10°C, light; 13 h, 20°C, light; 1 h, 20°C, dark; 9 h, 10°C, dark; light = 40 µmol m<sup>-2</sup> s<sup>-1</sup>). After hypocotyl emergence the temperature was increased (1 h, 15°C, light; 13 h, 25°C, light; 1 h, 25°C, dark; 9 h, 15°C, dark; light = 40 µmol m<sup>-2</sup> s<sup>-1</sup>). When hypocotyl > 2.5 cm the seed coat was removed and seedling transferred to hydroponics system. Seedlings were grown under axenic conditions at 25°C under light intensity of 40 µmol m<sup>-2</sup> s<sup>-1</sup> and a photoperiod of 14 h : 10 h, light : dark.

### Labelling experiments

Six- or seven-week-old seedlings were transferred to woody plant medium containing filter sterilised D-Glucose/D-Glucose-<sup>13</sup>C<sub>6</sub> or mevalonolactone/mevalonolactone-2-<sup>13</sup>C (2.5 mM). Three biological replicates were used for each experimental condition. After 3 wk of incubation, leaf, stem and root tissues of the plants were rinsed with water, frozen in liquid nitrogen and stored at -70°C until extraction.

### Phylogenetics

Immature leaf tissue was harvested onto dry ice. DNA-depleted RNA was isolated using a Direct-Zol RNA miniprep kit (Zymo Research, Irvine, CA, USA). RNA quantity and quality were assessed using the Agilent Tapestation system with RNA nano

screentape. For short read sequencing, library preparation was performed from 200 ng high quality total RNA input using the NEBNext Ultra II Directional Library prep kit for Illumina in conjunction with the NEBNext Poly(A) mRNA Magnetic Isolation Module and unique dual index set (New England Biolabs, Ipswich, MA, USA), according to the manufacturer’s instructions. Libraries were pooled at equimolar ratios and sent for paired end 150 base sequencing at Novogene (UK) Company Ltd. on a NovaSeq 6000 instrument (Illumina, San Diego, CA, USA), with 10 million reads per sample on average. *De novo* transcriptomes were assembled from reads using TRINITY including trimmomatic with default settings. Markers (rbcL, psbA, MatK, 5.8S) were identified in the transcriptomes using a local BLASTN search. All queries matched to full-length contigs except plant D matK which was split across two contigs which were concatenated to obtain the full-length matK marker. Marker sequences were obtained from the NCBI GenBank database by searching for taxonomy (Genus: *Daphniphyllum*), with *Cercidiphyllum japonicum* selected as an outgroup. Nucleotide sequences were aligned using MAFFT on default settings and maximum likelihood phylogenetic trees inferred using IQTree including ModelFinder on default settings (Minh *et al.*, 2020). For the combined tree including all four markers, only samples with four markers represented were retained and four separate sequence alignments were concatenated. The tree inference was performed with separate models predicted for each marker using partitions.

### LC-MS analysis

Plant material was obtained from plants growing in the UK (see Table S2). Tissues were sampled in triplicate onto dry ice before storing at -70°C. Plant material was freeze dried and ground with pestle and mortar. Samples (*c.* 10 mg) were extracted with 80% methanol (500 µl), vortexed, shaken in a TissueLyser (Qiagen) (10 min, 5 Hz) and then centrifuged (4000 g, 2 min). Supernatant (50 µl) was diluted with 80% methanol (450 µl) and added to a 96 well plate. The plates were sealed and stored at 4°C.

LC-MS/MS runs were performed using a Waters Acquity I-Class ultra performance liquid chromatography (UPLC) instrument interfaced to a Thermo Tribrid Fusion Orbitrap instrument using an atmospheric pressure chemical ionisation (APCI) ion source in positive ion mode. UPLC runs were controlled by WATERS EMPOWER software. 2-µl injections were made onto an Acquity BEH C18 column (100 × 2.1 mm, 1.7 µm particle size), held at 60°C. The column was run at 0.5 ml min<sup>-1</sup> with mobile phase A = 10 mM ammonium bicarbonate (pH 10.2) and B = MeOH. LC-MS data was processed with XCMS (3.12.0) and CAMERA (1.33.3) (Kuhl *et al.*, 2012) to identify features. Normalisation was performed using the R METMSLINE (1.2.1) package. Detailed description of LC-MS/MS methods and processing can be found in the Methods S1.

### Molecular networking

A molecular network was created using the Feature-Based Molecular Networking (FBMN) workflow (Nothias *et al.*, 2020) on

GNPS (<https://gnps.ucsd.edu>; Wang *et al.*, 2016) using default settings (see Methods S1). The GNPS network file was used as an input for SNAP-MS (Morehouse *et al.*, 2023) using the Cocnut reference database (Sorokina *et al.*, 2021) and default parameters. Molecular clusters with SNAP-MS derived *Daphniophyllum* alkaloid annotations were determined by manual inspection of SNAP-MS output. The alkaloid annotations were classified by type/subtype through manual inspection of structure or cross-reference of compound name with our curated alkaloid database.

## Compound clustering

For the initial multi-plant analysis, the loess corrected filtered peak areas were further filtered by removing values where peaks were only detected in one of three technical repeats, and removing features after 4.33 min. Next, all peak values for peaks whose maximum value fell below the median of all peak maxima were removed. The average and log-transformed LC-MS peak areas were calculated from technical repeats. The peak areas were then normalised across all samples by dividing the averaged and transformed peak areas by root-mean-square value across all samples for a given peak ( $\text{scale}(\text{centre} = \text{F})$  function in R). To describe changes of a group of peaks in a given sample, we used a cluster enrichment (CE) value, the sum of normalised peak areas within a given group. Averaged and log-transformed LC-MS peak areas were used for determining abundance cluster method, with the overall method using principal component analysis followed by UMAP (McInnes *et al.*, 2018) followed by clustering. The following hyperparameters were tested using a grid search: UMAP components, UMAP neighbours, and number of Principal Components. Two different hierarchical clustering methods were used: complete or median. Consensus clustering with 20 starts was always used for K-means clustering (Xiang *et al.*, 2021). The clustering methods were compared to ground-truth using *a priori* clusters by Rand-index (RI) and adjusted Rand-index (ARI). For compound clustering, the ground-truth *a priori* clusters were molecular cluster index from the FBMN GNPS network based on HCD composite MS<sup>2</sup> spectra. The cluster method selected was chosen based on a compromise between high ARI, to maximise confidence in cluster assignment, and number of clusters ( $k$ ), to maximise resolution.

## Cluster quantification

To describe the subtype annotation within each compound cluster (CC) we calculated a compound subtype score for each annotated peak based on the proportion of ambiguous/redundant annotations with particular subtypes. Each peak has a total score of one, but this is divided proportional to the annotations. For example, a peak annotated with three yuzurimine subtype compounds and one calciphylline A subtype compound would be scored 0.75 yuzurimine and 0.25 calciphylline A. To assign a subtype frequency across all peaks in a CC, these proportional subtype scores were summed. For the plant F only metabolomics experiment, average and log-transformed LC-MS peak areas were

calculated from loess corrected technical repeats. The peak areas were then normalised across all samples by dividing the averaged and transformed peak areas by root-mean-square value across all samples for a given peak ( $\text{scale}(\text{centre} = \text{F})$  function in R). Subtype enrichment (SE) across tissues was calculated by multiplying the proportional subtype score for each peak by the normalised peak area, summing these values across each sample, then scaling these values across all tissues ( $\text{scale}(\text{centre} = \text{T})$  function in R) for each biological replicate. These values represent the relative subtype enrichment (SE) across tissues in a sample.

## Methods for isotope labelling experiments

For the glucose labelling experiment, the LC-MS was run as described above. Feature picking was conducted as previously described but with a signal-to-noise threshold of 3 instead of the default 10. Features were matched against the in-house alkaloid database. Groups of features that may represent labelled compounds were selected by identifying pairs of features within  $\pm 2$  s RT tolerance and within  $\pm 0.05$   $m/z$  of <sup>13</sup>C mass increments were selected. These groupings were filtered to retain pairs where the ratio of the potentially labelled partner in a pair (i.e. the higher  $m/z$  value) is at least  $100 \times$  higher in labelled samples compared to control or unlabelled samples.

Peaks areas were then normalised by sample mass and filtered so only peaks with major (unlabelled) peaks  $> 10\,000$  were retained. Isotopolog proportion was calculated by dividing isotopolog peak area by the major (unlabelled) peak area. Corrected isotopolog proportions were calculated by subtracting average background isotopolog proportions (i.e. from samples fed with unlabelled precursors). Peaks were grouped by alkaloid type and number of <sup>13</sup>Cs incorporated. These populations were compared using ANOVA followed by Tukey's *post hoc* test.

For the mevalonolactone labelling experiment, the nine largest peaks in the unlabelled analysis were selected ( $5 \times \text{C30}$  type and  $4 \times \text{C22}$  type). For each peak, isotopolog peaks were identified within  $\pm 2$  s RT. Peaks areas were then normalised by sample mass, and grouped by alkaloid type and number of <sup>13</sup>Cs incorporated. Normalised isotope proportion was calculated by dividing isotopolog peak area by the major (unlabelled) peak area and normalised across each sample using Z-score. These populations were compared using ANOVA followed by Tukey's *post hoc* test.

## Microscopy

Tissue segments of stem, petiole and roots ( $\approx 0.5$  cm<sup>2</sup>) were cut, embedded in 15% gelatine, mounted to a holder using Tissue-Tek O.C.T compound, and sectioned (at  $-20^\circ\text{C}$ ) to a thickness of 40 to 80  $\mu\text{m}$  by Leica CM950 Cryostat (Leica Biosystems, Wetzlar, Germany). Suitable sections were mounted to SuperFrost Plus adhesion glass slides. To identify the major cell types in *Daphniophyllum* tissues the prepared sections were stained with Toluidine blue O (0.02% w/v) or Safranin O (1% w/v) and fast green (1% w/v) and then examined under bright-field microscopes (Nikon Eclipse E600, and Leica MZ16; Leica microsystems, Wetzlar, Germany).



## MALDI-MS analysis

Tissue sections (as prepared above) were sprayed with 40 mg ml<sup>-1</sup> 2,5-dihydroxybenzoic acid matrix in aqueous 50% methanol, 0.1% and MALDI-MS data acquired using a Waters SYNAPT G2-Si qTOF mass spectrometer with positive ionisation. Spectra were acquired with a 25 µm spatial resolution. Instrument control, data acquisition, and processing were performed using WATERS HDI software (v.1.5). The data were further processed using a python script (BASIS) (Veselkov *et al.*, 2018). The high mass accuracy LC-MS data was used as a reference for the selection of relevant peaks. Alkaloids with the highest log<sub>2</sub> value of the abundance across plant *F* samples were selected to investigate their distribution using MS imaging. Pearson-product moment correlations between the ion images of interest were calculated using HDI software (v.1.5), the obtained correlation matrix was used to build clustered heatmaps via the `heatmap` function in RSTUDIO using default settings (hierarchical clustering). Further details of the method in [Supplementary Information](#).

## Results

### Untargeted metabolomics annotation and clustering workflow

We set out to identify the variation in *Daphniphyllum* alkaloids (DAs) across different *D. macropodum* individuals and tissues. We obtained *D. macropodum* samples from multiple individuals (A–G) representing a range of ages, native geographic origin and tissues (Tables S2, S3). Due to limited access to chemical standards and the complex nature of the samples, we employed multiple complementary approaches to analyse the data. These included the use of MS<sup>1</sup>-based annotations, guided clustering, and MS<sup>2</sup>-based molecular networking (Fig. 2a).

### Peak networks and annotations

To annotate peaks based on MS<sup>1</sup> exact mass (i.e. chemical formula), we curated an *in silico* database of *Daphniphyllum* metabolites, consisting 331 *Daphniphyllum* alkaloids (DAs) which were categorised by subtype based on the carbon skeleton (Fig. S1; Table S4) (Chattopadhyay & Hanessian, 2017). These subtypes, in turn, were assigned as C30, C22B or C22A types (Figs 1a, S1A). Of 889 filtered peaks identified across the samples, 267 were annotated as DAs using this database. A limited number of peaks were annotated from chemical standards and MS<sup>2</sup> fragmentation data (Table S1). Feature-based molecular networking, which clusters peaks based on MS<sup>2</sup> fragmentation similarity, was conducted using the Global Natural Product Social Molecular Networking platform (GNPS) (Wang *et al.*, 2016; Nothias *et al.*, 2020). Of 51 molecular clusters (MCs) containing three peaks or more, 17 of these contained three or more DAs, according to MS<sup>1</sup>-annotations (Fig. S2). Furthermore, certain DA subtype annotations were associated with specific MCs, indicating a structural basis for molecular clustering (Fig. S3).

To validate our MS<sup>1</sup> annotation approach, we compared annotations to those generated by the Structural similarity Network Annotation Platform for Mass Spectrometry (SNAP-MS), an MS<sup>2</sup> network-based annotation approach, which we used to match MCs to chemical groups in the Coconut natural product database (Sorokina *et al.*, 2021; Morehouse *et al.*, 2023). SNAP-MS found six DA related MCs, of which five showed similar subtype classifications to our MS<sup>1</sup> annotations (Fig. S4). This validation encouraged us to persevere with the MS<sup>1</sup> annotation method in the absence of DA standards.

### Peak clustering and plant distribution

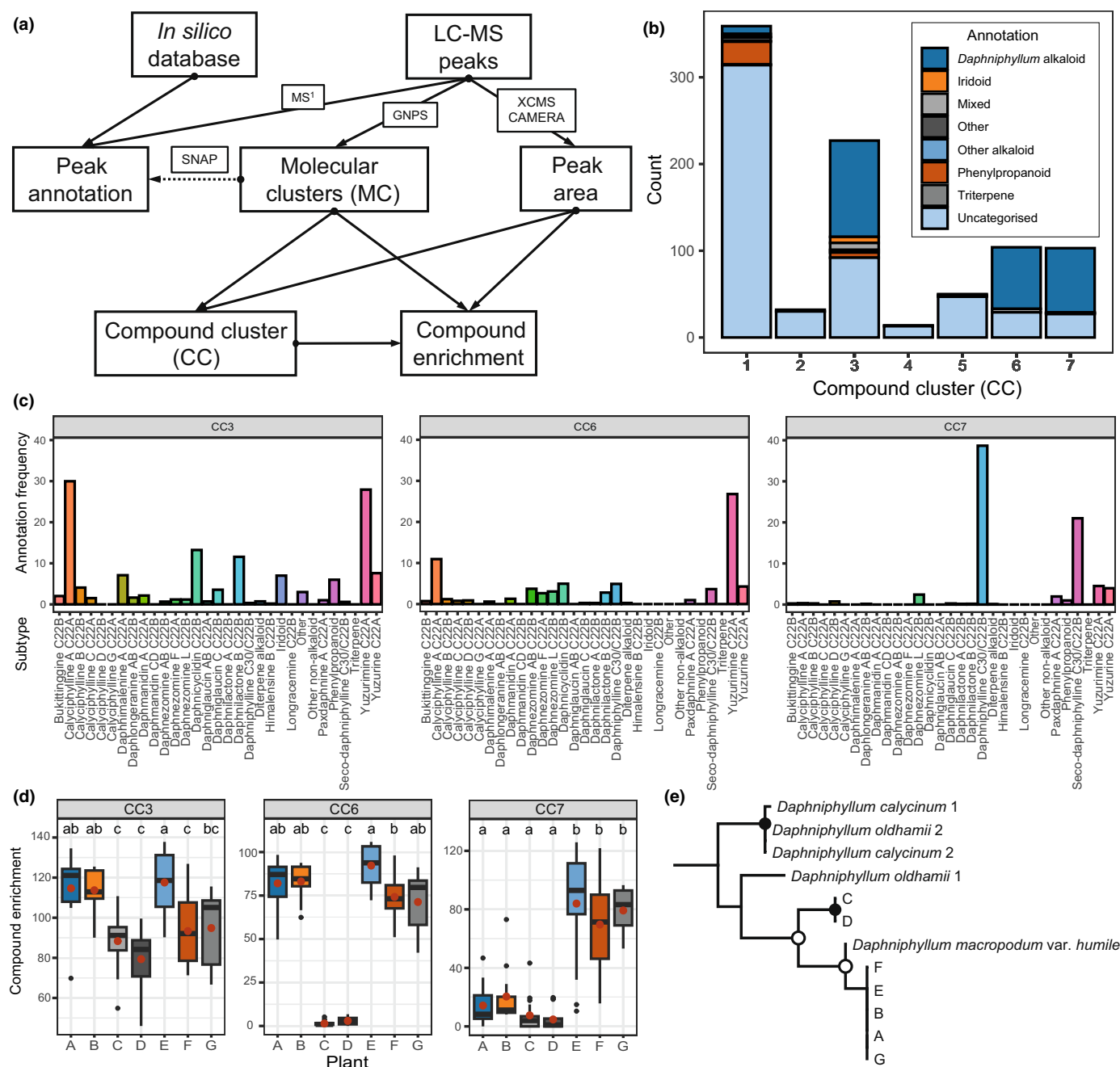
To identify groups of structurally related compounds whose presence correlated across samples, we used abundance (i.e. peak area) clustering method guided by MCs. First, we reduced the dimensionality of the abundance data using principal component analysis (PCA) and Uniform Manifold Approximation and Projection (UMAP), and then iterated through cluster algorithms and parameters to identify a clustering method that best replicated MC relationships, adjusting for chance grouping and desired cluster number (Fig. S5). The selected method had seven compound clusters (CC), three of which (CCs 3, 6 and 7) contained large numbers of peaks annotated as DAs (Fig. 2b).

DA subtype annotations were unequally distributed across CCs: CC7 contained mostly daphniphylline and secodaphniphylline subtypes, CC6 contained mostly yuzurimine subtypes and CC3 contained a mixture of C22 subtypes, with yuzurimine and calyciphylline A subtypes most represented (Fig. 2c). To assess the distribution of these CCs across different plants, we limited the analysis to peaks annotated as DAs and tissue types that were represented from all plants (immature leaf, mature leaf and petiole) and used a metric (compound enrichment) to assess the relative abundance of groups of chemicals across tissues. This showed that CC3 DAs were most abundant in plants A, B and E; CC6 DAs were significantly low in plants C and D; and CC7 DAs were enriched in plants E, F and G (Fig. 2d).

By inspecting MCs (MS<sup>2</sup>-based molecular clusters) associated with specific CCs (abundance-based compound clusters), we could gain a higher resolution description of alkaloid distributions across plants (Fig. S6). Multiple MCs (i.e. 26, 35, 72, 109) associated with CC3 were annotated as calyciphylline A/yuzurimine subtypes (Fig. S3) and were well represented across all plants. MCs 23 (yuzurimine subtypes) and 61 (daphnezomine F subtypes), represented in CC6, were significantly low in plant C and D. MCs 16, 28, 48 and 77, associated primarily with CC7 and annotated as secodaphniphylline or daphniphylline subtypes, were significantly high in plants E, F and G.

### Genotypes

To assess whether the genotype correlated with DA content, we obtained *de novo* transcriptomes from each plant, identified marker genes, and performed phylogenetic analysis (Figs 2e, S7; Table S5). Plants C and D are genetically distinct from the other plants, which matches their different geographic origin



**Fig. 2** Multi-plant untargeted metabolomics analysis of *Daphniphyllum macropodum*. (a) Workflow employed for analysing untargeted LC-MS data. Solid arrows denote transfer of information/data; dotted arrow represents validation step. Acronyms on arrows represent data type or software employed. (b) Distribution of annotations in compound clusters (CC). (c) Peak subtype annotations in compound clusters one, six and seven, using proportional subtype annotations where multiple annotations are counted as a fraction of a count. (d) Distribution of CCs across different plants (limited to immature leaf, mature leaf and petiole). Red dots show mean values alongside standard boxplots (outliers, black dots; whiskers, 0<sup>th</sup> or 100<sup>th</sup> percentile; box, lower and upper quartiles; line, median). Letters above boxplots show significant groups as determined by Dunn *post hoc* test following a Kruskal–Wallis test with Benjamini–Hochberg correction. (e) Phylogenetic tree showing genotype relationships of plants using four marker genes. Solid dots on nodes show very high branch support (SH-aLRT > 90, ultrafast bootstrap > 95), hollow dots show good branch support (SH-aLRT > 90, ultrafast bootstrap > 90), no dots show low supported branches (SH-aLRT < 90, ultrafast bootstrap < 90). Further details of phylogenetics can be found on Supporting Information Fig. S7.

(Table S3). The alkaloids in CC6 appear to be impacted by genotype as they are very low in plants C and D but present in A and B, despite all being mature plants growing in the same woodland (Fig. 2d; Table S3). However, alkaloids in CC7 appear more

influenced by age or growth conditions than genotype: plants A, B, E, F and G are genotypically identical (Fig. 2e) yet the young (<5 yr) potted plants E, F and G have significantly greater enrichment in CC7 alkaloids than mature plants A and B

(Table S3; Fig. 2d). Sex does not appear to be a major influencing factor as male/female pairs of similar plants (i.e. A/B and C/D) show similar alkaloid content.

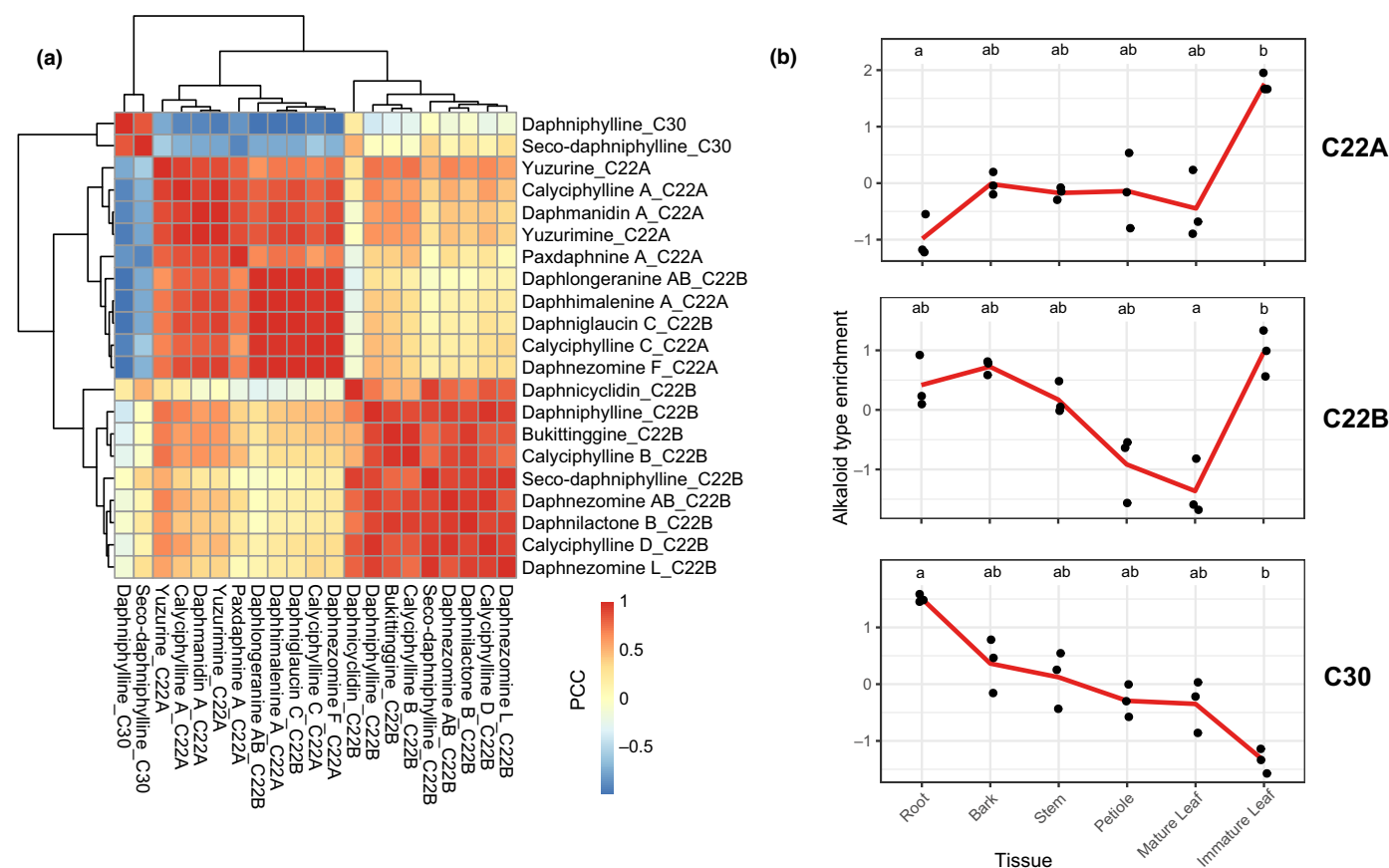
### Tissue distribution

Using the same dataset, we assessed CC distributions across tissue types, excluding the genetically and metabolically divergent plants C and D. We found that CC3 DAs were highest in flowers, fruit, immature leaf and leaf bud (Fig. S8A). There were no significant differences of CC6 across tissues. CC7 DAs were generally higher in older or woodier tissue (i.e. mature leaf, petiole, root). The constituent MCs largely followed the same trend as the CCs (Fig. S8B). There was high accumulation of yuzurine subtypes (MC 112 and 118) in leaf bud and flowers, and of daphnilactone B subtypes (MC 62) in fruit and flowers (Figs S3, S8B). Daphniphylline subtypes (MC 16 and 77), only represented in CC7, showed high enrichment in roots and mature tissues and near/below the limit of detection in flowers and leaf buds. Overall, this multi-plant, multi-tissue analysis provides

evidence that plant genotype and tissue influence the accumulation of DA subtypes.

To understand more thoroughly the distribution of DAs across tissues, we performed metabolomics on three plants from a single taxon and geographical origin (plant F) (Tables S2, S3; analysis 2; Fig. S9). The DA subtypes showed distinct patterns across tissues, largely correlating with whether the subtypes were C30, C22A or C22B type alkaloids (Figs 3a, S10; Table S6). In fact, when grouped in this manner, distinct and significant distributions across tissues are observed (Fig. 3b; Table S6). C30 DAs are relatively high in roots and low in immature leaves. C22B alkaloids are high in immature leaves, lower in mature leaves but relatively evenly distributed across roots, stem and bark. C22A DAs are high in immature leaves and low in roots.

To validate that the tissue distribution of DAs was not specific to plant F, we analysed the leaves and roots of three seedlings derived from plant B seed (Tables S2 and S3, analysis 3), selected the top five differential peaks between roots and leaves, and found them to have the same tissue distribution pattern as equivalent peaks in the plant F analysis (Fig. S11).



**Fig. 3** Distribution of alkaloid subtypes across *Daphniphyllum macropodum* tissues. (a) Correlation of subtypes across tissues. Subtype enrichment values (see the **Materials and Methods** section, Supporting Information Fig. S10; Table S6) were compared using Pearson correlation coefficients (PCC), depicted in a heatmap and clustered with hierarchical clustering represented by the dendrograms. Note the hierarchical clustering largely recovers C30, C22B and C22A type groupings. (b) Distribution of *Daphniphyllum* alkaloid types across tissues. Points represent biological replicates of subtype enrichment values. Red line connects mean values. All types show significant variation across tissues (Kruskal–Wallis tests,  $P < 0.05$ , Table S6). Letters represent grouping in Dunn *post hoc* tests (Table S6).

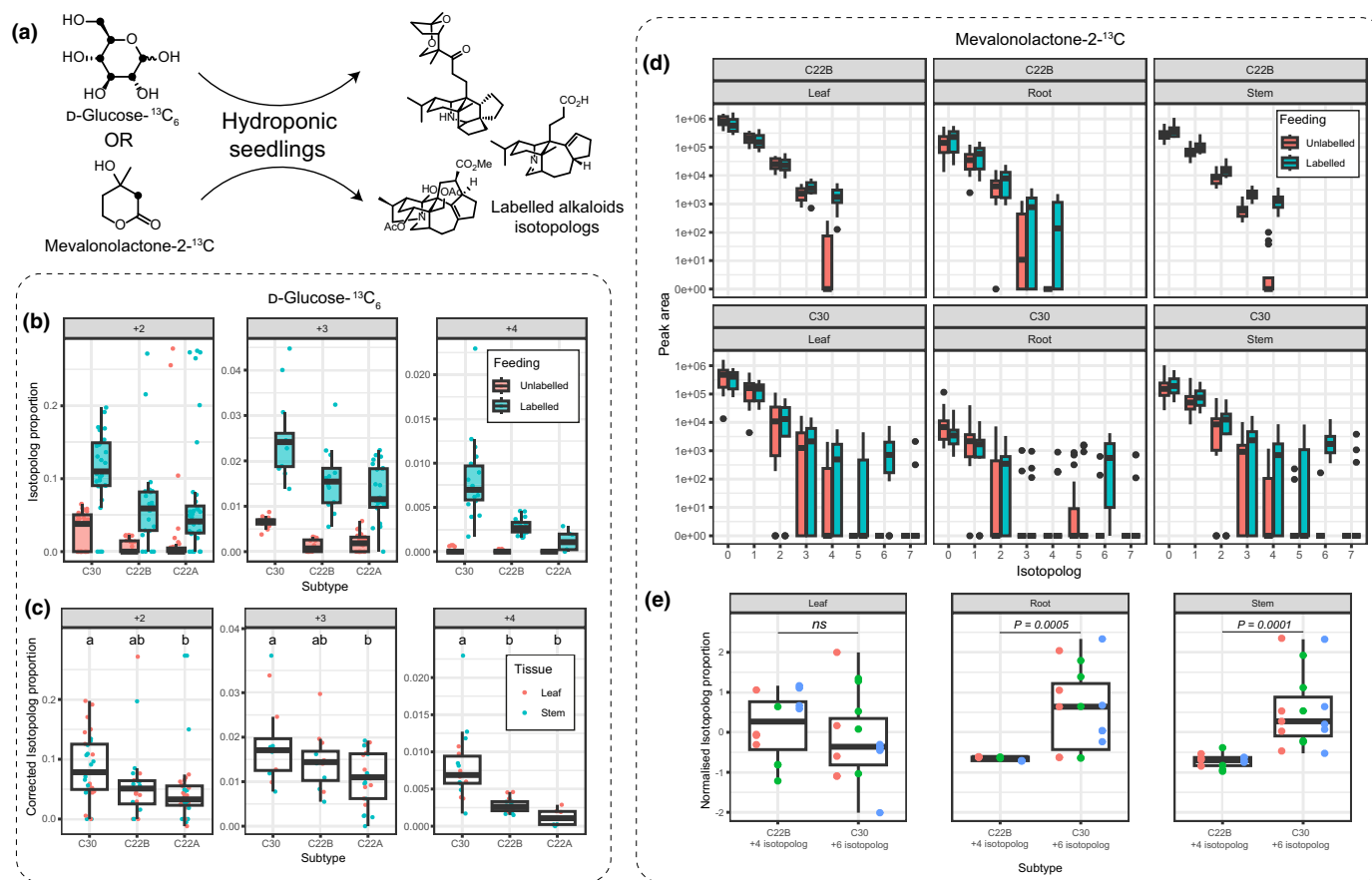


## Isotope labelling studies

Previous studies employed radioactive isotope labelling of DAs to determine that they are terpenoid in origin (Niwa *et al.*, 1973; Suzuki *et al.*, 1973). We used stable isotope precursor feeding of hydroponic seedlings followed by metabolomics to probe the biosynthetic origins of the DAs (Fig. 4a). In the leaves and stem of samples fed with  $^{13}\text{C}_6$ -glucose we found increases in DA isotopologs (+2 to +4) compared to samples with fed with unlabelled glucose (Fig. 4b; Sample details in Table S2; analysis 4). Correcting for natural isotopolog abundance, we assessed the proportion of heavy isotopolog peaks compared to the unlabelled peak across the DA types C30, C22B and C22A (Fig. 4c). We found that isotopolog proportions were significantly higher in C30 compared to C22A (+2,  $P = 0.03$ ; +3,  $P = 0.007$ ; +4,  $P = 0.0006$ ).

C30 type alkaloids also showed significantly higher +4 isotopolog proportions than C22B ( $P = 0.00004$ ). The higher isotopolog proportion indicates higher *de novo* biosynthesis during the isotope feeding regime, and therefore suggests that C30 compounds are biosynthesised before C22B and C22A subtypes.

We then performed a feeding experiment with mevalonolactone-2- $^{13}\text{C}$  (Fig. 4a, Sample details in Table S2, analysis 5). We selected the nine most abundant alkaloid peaks for analysis (five C30s and four C22Bs) across all leaf, root and stem tissues. In all tissues, these peaks showed an increase in heavy isotopologs upon labelled precursor feeding (Fig. 4d). C22B type alkaloids showed greatest proportional increase at +4, with no heavier isotopologs identified for those compounds. By contrast, C30 compounds showed greatest proportional increase at +6. This difference reflects the isoprene ( $\text{C}_5$ ) units that make up the carbon skeleton, derived from



**Fig. 4** Stable isotope labelling experiments in *Daphniphyllum macropodum*. (a) Overview of experimental set-up: labelled precursors are fed to hydroponic seedlings and alkaloid content is analysed. (b) Glucose- $^{13}\text{C}_6$  labelling experiment showing isotope proportion (isotopolog peak area/natural isotopolog peak area), across +2, +3 and +4 peaks, separated by peak subtype annotation. Only leaf and stem are included. Each point represents a single compound from a single sample; three biological repeats each for labelled and unlabelled are represented. (c) As in (b) but showing corrected isotope proportion (isotope proportion in a labelled sample – mean of isotope proportion in three unlabelled samples). Letters represent groups determined by ANOVA and Tukey's *post hoc* test ( $P < 0.05$ ). (d) Mevalonolactone-2- $^{13}\text{C}$  labelling experiment showing peak areas of nine most abundant peaks. Y-axis shows peak area with log scale. X-axis shows positive isotopolog peaks, with zero the naturally highest abundance isotopolog. Peaks > +4 not observed for C22 compounds. (e) Normalised isotope enrichment (isotope proportion normalised across samples by Z-score) for C22B (+4 isotopolog) and C30 (+6 isotopolog) compounds. Three biological replicates examined; only labelled samples depicted. Points with the same colours are derived from the same replicate. Each point represents a compound from a single sample; selected compounds were the same as in (d). Significance of difference of means (*t*-test,  $P$ -value). All boxplots: outliers, black dots; whiskers, 0<sup>th</sup> or 100<sup>th</sup> percentile; box, lower and upper quartiles; line, median. In (b, c, e) all individual data points are shown as coloured points; in (d, e) only outliers are shown as black points.

mevalonate via squalene, validating observations in previous labelling experiments (Niwa *et al.*, 1973; Suzuki *et al.*, 1973).

As in the glucose labelling experiment, the degree of isotopolog enrichment was influenced by the alkaloid type. In roots and stem, the C30 alkaloid demonstrated significant +6 normalised isotopolog proportions compared to the +4 isotopolog enrichment of C22B compounds ( $P = 0.0005$  and  $P = 0.0001$  for root and stem, respectively) (Fig. 4e). This further supports that C30 compounds are earlier than C22B compounds in the pathway from mevalonate, supporting established biosynthetic logic.

### Mass spectrometry imaging

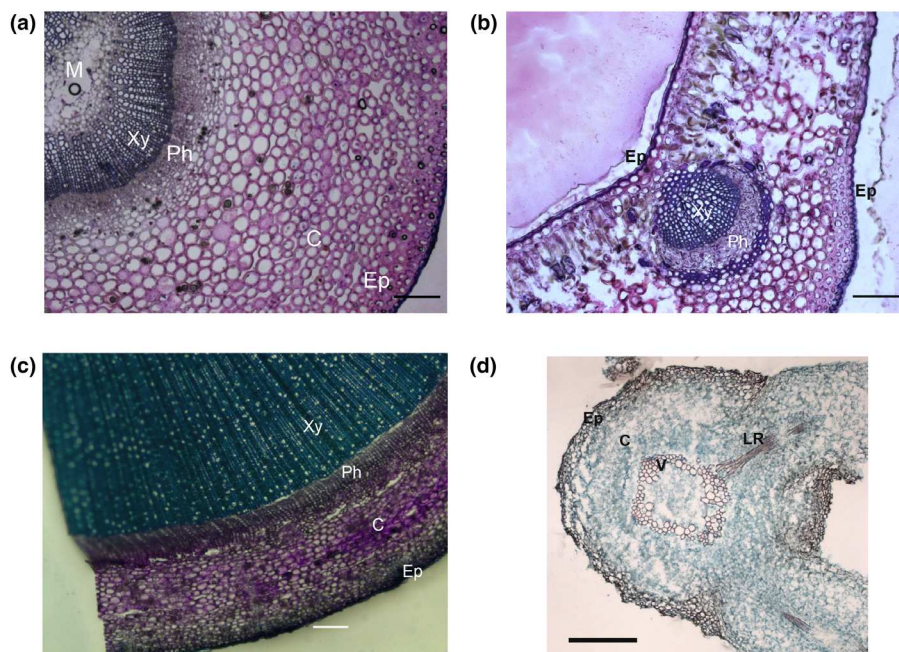
Having established that DA subtypes vary between different tissues, we set out to investigate the spatial distribution of DAs within specific tissues. First, we characterised the tissue structure using microscopy (Fig. 5). We examined petioles (Fig. 5a), leaves (Fig. 5b), stems (Fig. 5c), and immature roots (Fig. 5d) and identified the main structures of tissues. We then used matrix-assisted laser desorption/ionisation MS (MALDI-MS) to detect compound distribution within those tissue regions. We focused on representative alkaloids that were highly abundant in plant F according to the LC-MS analysis.

The MALDI-MS analysis of a petiole cross section revealed distinct spatial distribution of DAs, with alkaloids detected with high intensity in the epidermis, phloem region, and the medulla (Figs 6a–d, S12A; Table S7). A subset of ions, including  $m/z$  370.2333 and 372.2513 (C22A), were located exclusively to the epidermis region. Other ions such as  $m/z$  470.3621 and 486.3571 (C30), were readily detected with high intensity in the phloem region, medulla and epidermis (Fig. 6c). A third pattern was also observed for alkaloids including  $m/z$  512.3707 and

528.3670 (C30), these were most abundant in the phloem region and medulla whilst largely absent in the epidermis (Fig. 6d).

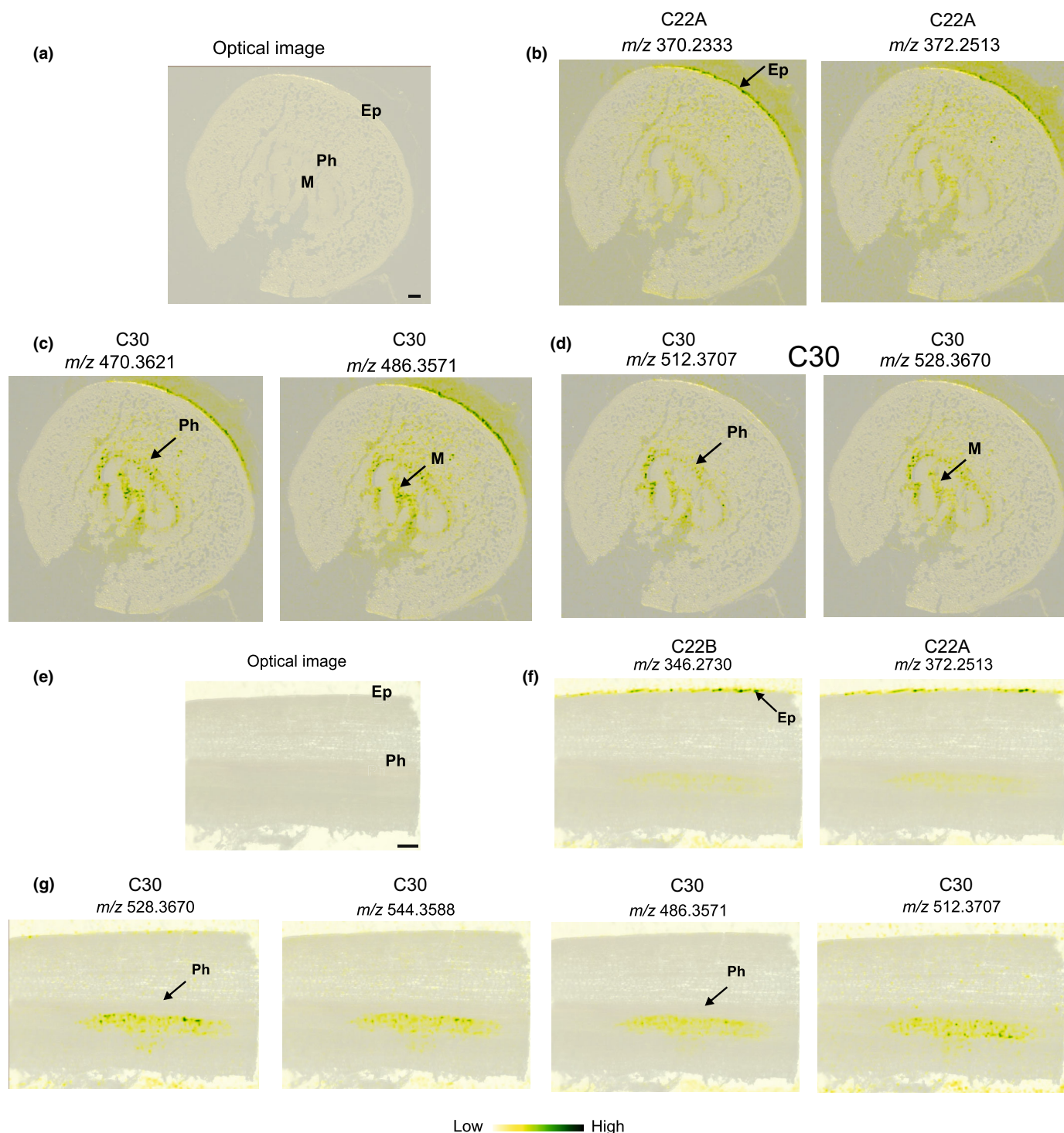
Further examination of alkaloid localisation in a longitudinal stem section showed similar trends, with the alkaloids detected in the epidermal cells and the phloem region (Figs 6e–g, S12B; Table S7). For instance, the molecular ions  $m/z$  346.2730 (C22B) and 372.2513 (C22A) were distributed mostly in the epidermal cells and to a lesser extent in the phloem. Molecular ions of C30 type, including  $m/z$  472.2658, 486.3571, 528.3670 and 544.3588 were detected mostly in the phloem region. (Table 1). A stem cross section image also provided a similar contrast in compound distribution (Fig. S12C). Assessment of seedling roots with imaging-MS also showed alkaloid masses associated with the phloem or epidermis, but alkaloid abundance was too low to observe a great range of compounds (Fig. S13).

For specific MS images, we generated spatial correlation values and a heatmap, which highlighted groups of spatially correlated compounds (Fig. S14). When we inspected the annotation of these alkaloids based on LC-MS peaks of matching mass known from these samples, we noticed that C22A and C22B DA distributions tended to cluster together, indicating co-localisation in the analysed cross sections, whereas C30 DAs tended to form a distinct cluster. Tabulation of  $m/z$  observations across three images similarly shows a pattern of intra-tissue distribution related to DA type (Table 1). Therefore, it appeared that compounds belonging to C22A and C22B tend to localise to the epidermal cells, while alkaloids belonging to C30 tend to localise in the phloem region. However, whilst showing trends, compounds were not found exclusively in one region, but vary across these regions in abundance and show slightly different patterns between samples. The exception to this were the three strictly phloem specific C30 masses ( $m/z$  544.3588, 512.3707, and 528.3670).



**Fig. 5** Micrographs of *Daphniphyllum macropodum* tissues cross sections. (a) Petiole stained with Toluidine blue O. (b) Leaf stained with Toluidine blue O. (c) Stem stained with Toluidine blue O. (d) Seedling root stained with Safranin O/Fast Green. Positions of the different cell types are indicated: medulla (M), phloem (Ph), cortex (C), epidermal cells (Ep), xylem (Xy), vascular cylinder (V) and lateral roots (LR). For (a, b, c), Bar, 200 µm; for (d), Bar, 100 µm.





**Fig. 6** Distribution of alkaloids within petiole and stem tissue of *Daphniphyllum macropodum*. Ion intensity maps of selected alkaloids detected as  $[M + H]^+$  ions with the MALDI-MS in the cross section of *D. macropodum* petiole (a–d) and longitudinal section of *D. macropodum* stem (e–g). Micrographs included for comparison (a, e, size bar = 200  $\mu$ m), which are also added as background to the MS images. Colour bar represents MS signal intensity. Positions of the epidermis (Ep), the phloem region (Ph), and the medulla (M) are indicated. The different panels indicate patterns of DA distributions with enrichment in the epidermis (b, f), phloem/medulla (d, g) or all locations (c). MALDI-MS analysis of a stem cross section provided similar results (Supporting Information Fig. S11). Alkaloid type designation placed above mass value; see Table 1 for collected data.

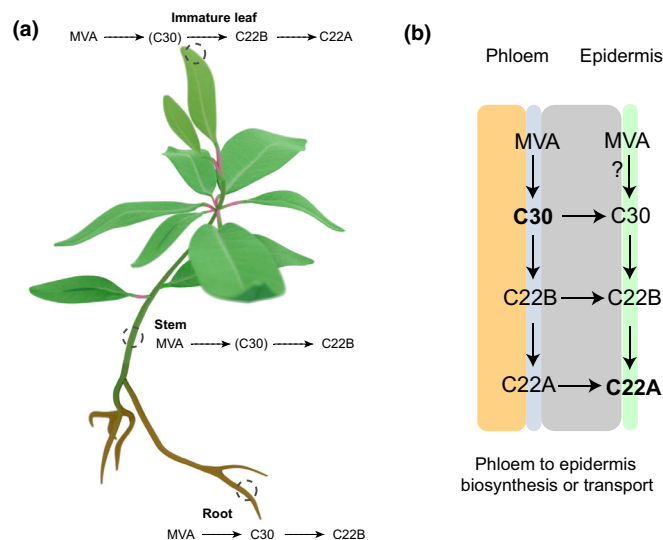
The spatial distribution of DA subtypes within tissues determined by MALDI-MS mirrors patterns of distribution between tissues determined by LC-MS. In the initial LC-MS analysis we

found CC7 compounds, of C30 daphniphylline and secodaphniphylline subtype, associated with organs containing vascular tissue, whilst yuzurimine subtype C22A/CC6 compounds

**Table 1** Localisation of alkaloids in *Daphniphyllum macropodum* tissues.

MALDI Measured <i>m/z</i>	LC-MS Peak ID	Type	Epidermis			Phloem		
			P	S1	S2	P	S1	S2
368.217	M368.2223T188	C22A	✓✓	✓✓	✓✓	✓		
370.2333	M370.2380T176	C22A	✓✓	✓✓	✓✓	✓		
372.2513	M372.2537T251	C22A	✓✓	✓✓	✓✓	✓	✓	
414.2611	M414.2644T209	C22A	✓✓	✓	✓✓	✓	✓	✓
472.2658	M472.2698T207	C22A	✓✓	✓	✓✓	✓	✓	✓
386.2364	M386.2330T170	C22A	✓✓		✓✓			
342.2426	M342.2430T157	C22B	✓✓	✓✓	✓✓	✓	✓	
374.2678	M374.2693T122	C22B	✓✓	✓	✓✓	✓	✓	
376.2856	M376.2849T263	C22B	✓✓		✓✓	✓		✓✓
346.273	M346.2743T156	C22B		✓✓	✓✓		✓	
360.2573	M360.2536T65	C22B			✓✓		✓	
362.2674	M362.2693T81	C22B			✓✓		✓	
470.3621	M470.3633T312	C30	✓	✓		✓	✓✓	✓✓
502.3462	M502.3532T223	C30	✓		✓	✓	✓✓	✓
472.3722	M472.3790T273	C30	✓			✓✓	✓✓	✓✓
486.3571	M486.3584T253	C30	✓✓		✓✓	✓✓	✓✓	✓✓
512.3707	M512.3740T307	C30				✓✓	✓✓	✓✓
528.367	M528.3689T313	C30				✓✓	✓✓	✓✓
544.3588	M544.3640T261	C30				✓✓	✓✓	✓✓

Presence of *Daphniphyllum* alkaloids (DAs) in region determined by ion intensity maps. Compounds were judged to be abundant (✓✓), present (✓) or below the limit of detection (blank) based on visual assessment of ion intensity map (all available in Supporting Information Figs 6, S12). LC-MS peak IDs were determined by matching mass to the compound of highest abundance in plant F (Table S7). Three different images were assessed: petiole cross section (P), stem longitudinal cross section (S1) and stem cross section (S2).



**Fig. 7** Proposed organisation of *Daphniphyllum macropodum* alkaloid biosynthesis. (a) We propose alkaloids are biosynthesised in multiple tissues from mevalonate via C30 forms. (b) Cellular organisation of alkaloids, with C30 precursors primarily observed in the phloem and C22A compounds accumulating in the epidermis.

associated with younger, low-vascular tissue containing organs. Accordingly, the MALDI-MS images shows ions corresponding to C30 DAs associated with the vascular phloem tissue, whereas ions representing C22 DAs are enriched in the epidermis. Overall, the agreement between the independently conducted MALDI-MS and LC-MS experiments verifies that DA subtypes demonstrate distinct distribution in plants.

## Discussion

The *Daphniphyllum* alkaloids are a unique and diverse group of natural products. Their structural complexity has inspired total synthetic campaigns where cutting-edge chemical methods are employed alongside ingenious synthetic steps in an attempt to replicate nature's biosynthetic feats (Guo *et al.*, 2020a). There has been some, if limited, examination of DA bioactivities, but their polycyclic structures make them attractive for further exploration (Wu *et al.*, 2013). Isotope labelling experiments demonstrated the terpenoid origin of the alkaloids (Suzuki *et al.*, 1973) and landmark synthetic biomimetic syntheses demonstrated how squalene derived aldehydes could form the secodaphniphylline skeleton in mild conditions (Pietre & Heathcock, 1990). Despite this, much regarding the biosynthetic origins and biological role of alkaloids in *Daphniphyllum* species is unknown.

Understanding the spatial distribution of DAs will give insight into their biological function and arrangement of the biosynthetic pathway. To investigate this, we performed metabolomics analysis using a combination of mass spectrometry methods. A major challenge for the analysis was the lack of available standards: *in lieu* of chemical standards, we developed a workflow that combined MS<sup>1</sup> annotations, MS<sup>2</sup> networking and clustering (Fig. 2a). This method enabled us to analyse the large metabolomics dataset holistically without relying on ambiguous annotations of single peaks but instead using cumulative annotations across compound clusters. This workflow and clustering method can be generalised to other metabolomics datasets where standards are difficult to obtain.

The LC-MS analysis revealed DA subtypes vary across plants and organs. Plants C and D, originally from Guizhou province, China, accumulate different DAs compared to other plants investigated here, which either originate from Japan or European horticultural sources (Fig. 2d). Genetic analysis of C and D revealed them to be genetically distinct to the other plants, indicating a genetic contribution of chemotype diversity across the species (Fig. 2e). The age or growth conditions of the plants also have an influence on the accumulation of DAs (Fig. 2e).

By examining the DAs by structural annotation, especially whether they were annotated as C30 or C22 skeletons, and for the latter, whether a hexahydropentalene moiety was present (C22A) or absent (C22B), we revealed patterns of distributions (Fig. 3). All C22 compounds were enriched in immature leaves. There were also differences between C22A and C22B compounds, with the former comparatively low in roots, whereas the latter are present in roots but low in mature leaves. C30 compounds are enriched in roots and low in immature leaves. The results here match studies into *D. oldhamii*. Two *D. oldhamii* plants from different regions of Guizhou province were found to produce different subtypes DAs, with yuzurimine and daphniphyllidin subtypes showing differences between the individuals (Shuzhen *et al.*, 2013). Collation of data from natural product isolations of *D. oldhamii* also indicates DA subtypes are differentially distributed in organs, with yuzurimine subtypes extract primarily in leaves, (seco)daphniphylline subtypes in root and yuzurine subtypes in fruit (Mu *et al.*, 2008).

To examine the biosynthetic pathway of DAs, we employed isotope labelling, using either glucose- $^{13}\text{C}_6$  or mevalonolactone- $^{13}\text{C}$  precursors to feed hydroponic plants. Across both experiments we saw C30 DAs accumulating greater quantities of isotopes than C22 DAs (Fig. 4c, e), indicating C30s are metabolically closer to the precursors and precede the C22s in the pathway. Furthermore, the work verified previous work from Suzuki *et al.* by demonstrating the mevalonate (i.e. terpenoid) origin of DAs including the presence of six  $\text{C}_5$  isoprene units in C30 compounds and four in C22 compounds (Fig. 4d) (Niwa *et al.*, 1973; Suzuki *et al.*, 1973). Finally, across all experiments we identified labelling of C30 compounds in all three tested tissue types (leaf, stem, root) (Fig. 4d). This, alongside previous work by Suzuki *et al.* which shows labelling of C30 compounds in aerial tissues in the absence of roots (Suzuki *et al.*, 1973), indicates *de novo* biosynthesis in multiple tissues and not long-distance inter-tissue transport of alkaloids in as shown in the *Senecio vulgaris* pyrrolizidine alkaloid pathway (Ehmke *et al.*, 1988; Witte *et al.*, 1990).

The MALDI-MS imaging can complement metabolomic analysis of homogenised tissues in LC-MS (Dong *et al.*, 2016, 2020; Bednarz *et al.*, 2019). The ion intensity maps showed that DAs were localised in specific regions of the petiole and stem tissues (Figs 6, S14). Correspondence of MALDI-MS ions with LC-MS peaks provided access to compound cluster/subtype information (Table S7). The independently acquired MALDI-MS data validated the LC-MS work, with C30 subtypes preferentially associated with vascular tissue (phloem) and C22 subtypes preferentially localised to the epidermis.

In an ecological context alkaloid localisation within epidermal cells may suggest a role in defence, as the epidermis is the most exposed tissue to environmental stressors such as pathogens and herbivores. Epidermal cells have been found to accumulate alkaloids in other plants, such as quinolizidine alkaloids in lupin species (Wink, 1986), where they act to deter herbivores (Lee *et al.*, 2007). There is evidence that some DAs have insecticidal (Li *et al.*, 2009) or pesticidal (Cao *et al.*, 2012; Zhang *et al.*, 2013) bioactivities, though this has not been thoroughly explored. C22 subtype compounds that accumulate in the epidermis are also significantly enriched in immature leaf, a tissue that may be particularly at risk of attack as they have high nutritional value and may lack the waxy protective layer of mature leaves. Altogether, the localisation of C22 subtype DAs in the epidermis, and accumulation in immature leaf, suggests their role in defence against bioaggressors.

By considering the biosynthetic pathway alongside metabolite localisation and isotope labelling we can build a model of DA biosynthesis in the plant (Fig. 7). As all DAs are derived from squalene (C30), and likely pass through a single entry-point, C22 DAs must derive from one or more C30 DAs. Evidence of the pathway origin is found in the seminal syntheses by Pietre & Heathcock (1990) and Heathcock & Stafford (1992), which place the secodaphniphylline as the precursor to other subtypes. Notably, daphniphylline subtypes are not thought to be intermediates but end products in their own right (Heathcock & Joe, 1995; Mu *et al.*, 2008).

MS-imaging experiments show the C30 compounds are localised primarily in the phloem region, and therefore is likely where the first steps of DA biosynthesis are located (Fig. 7b). C22 compounds, especially C22A type like yuzurimine, are localised to the epidermis. Therefore, transport between these cell types may be occurring, though we do not know which compound types are translocated, as no compound type shows exclusive distribution. Alternatively the two regions may have fully localised exclusive pathways with different end-points. The mevalonate labelling experiments support previous labelling and biomimetic syntheses (Niwa *et al.*, 1973; Suzuki *et al.*, 1973; Mu *et al.*, 2008; Kobayashi & Kubota, 2009) showing the C30 DAs are formed from six isoprene units (i.e. squalene) with C22 DAs derived from these with loss of  $\text{C}_8$  and two isoprene derived labels.

In summary, we have employed metabolomics analysis to investigate the biological function and biosynthetic origins of *Daphniphyllum* alkaloids. Our analysis indicates that alkaloid distribution within the tissues is complex, with the likely involvement of intercellular transport. *Daphniphyllum* alkaloids have a remarkable skeletal diversity, and the structure dependent distribution discovered here represents a significant step forward in understanding their organisation and origin. The gained insights on the distribution of alkaloids in *Daphniphyllum* can guide further gene discovery efforts through examining gene expression across different cell and tissue types through, for instance, single cell RNA-Seq (Li *et al.*, 2023). Through future combination of metabolomics and genomic approaches, it may be possible to understand how *Daphniphyllum* constructs molecules of such remarkable complexity and variety.



## Acknowledgements

We acknowledge the University of York Biology Technology Facility, the Centre of Excellence in Mass Spectrometry, the Biology Horticultural Facility and the Chemistry NMR facility in conducting this research. We thank Karen Hogg and Clare Steele-King in the Biology Technology Facility for imaging mass-spectrometry support. We thank the Yorkshire Arboretum and Castle Howard for access to the plant material and to John Grimshaw and Jonathan Burton for support. We are grateful for Bledyn Wynn-Jones for taxonomic assignment. The work is supported through a UKRI Future Leaders Fellowship awarded to BRL (MR/S01862X/1 and MR/X010260/1). BAR is supported by a BBSRC White Rose DTP studentship (BB/T007222/1). We acknowledge a University of York Research Priming award for funding SC.








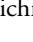
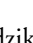
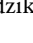
## Competing interests

None declared.

## Author contributions

KE and BRL conceived of the study, interpreted data and wrote the article. KE, CBW and DJT prepared samples. BAR and WPU isolated and characterised alkaloid standards. DJT performed microscopy and sectioning. SC, WD, and DE developed clustering workflow for untargeted metabolomics. SL performed LC-MS data acquisition. AAD performed imaging-MS data acquisition. SJ prepared sequencing libraries. TRL processed LC-MS and imaging-MS data. KE analysed imaging-MS data. BRL led the study. All authors read and approved the manuscript.

## ORCID

William Davis  <https://orcid.org/0000-0001-9267-5774>  
Adam A. Dowle  <https://orcid.org/0000-0002-6501-5444>  
Kaouther Eljounaidi  <https://orcid.org/0000-0003-4675-226X>  
Daphne Ezer  <https://orcid.org/0000-0002-1685-6909>  
Sally James  <https://orcid.org/0000-0003-2701-9724>  
Swen Langer  <https://orcid.org/0000-0002-9684-1167>  
Tony R. Larson  <https://orcid.org/0000-0003-1337-3482>  
Benjamin R. Lichman  <https://orcid.org/0000-0002-0033-1120>  
Barbara A. Radzikowska  <https://orcid.org/0000-0001-8706-3087>  
William P. Unsworth  <https://orcid.org/0000-0002-9169-5156>

## Data availability

For LC-MS/MS analysis the source data files including the collated .mgf file and other metadata are deposited at MassIVE with identifier MSV000093910 (doi: [10.25345/C5WP9TJ00](https://doi.org/10.25345/C5WP9TJ00)). MALDI-MS raw data files and derived HDI .txt files are available at MassIVE with identifier MSV000093919 (doi: [10.25345/C5R20S70P](https://doi.org/10.25345/C5R20S70P)).

The GNPS molecular networking job can be publicly accessed at <https://gnps.ucsd.edu/ProteoSAFe/status.jsp?task=a8b1a6fc87684bf99decae350513ea7c>. Reads for transcriptome analysis are available on NCBI Sequence Read Archive (PRJNA1067848). Sequences extracted for phylogenetic analysis are available on NCBI GenBank (ITS: PP227286-PP227292, matK: PP263638-PP263644, psbA: PP263645-PP263651, rbcL: PP263652-PP263658).

## References

- Augustin MM, Ruzicka DR, Shukla AK, Augustin JM, Starks CM, O'Neil-Johnson M, McKain MR, Evans BS, Barrett MD, Smithson A *et al.* 2015. Elucidating steroid alkaloid biosynthesis in *Veratrum californicum*: production of verazine in Sf9 cells. *The Plant Journal* **82**: 991–1003.
- Bednarz H, Roloff N, Niehaus K. 2019. Mass spectrometry imaging of the spatial and temporal localization of alkaloids in nightshades. *Journal of Agricultural and Food Chemistry* **67**: 13470–13477.
- Bharate SS, Mignani S, Vishwakarma RA. 2018. Why are the majority of active compounds in the CNS domain natural products? A critical analysis. *Journal of Medicinal Chemistry* **61**: 10345–10374.
- Bird DA, Franceschi VR, Facchinia PJ. 2003. A tale of three cell types: alkaloid biosynthesis is localized to sieve elements in opium poppy. *Plant Cell* **15**: 2626–2635.
- Boyce P. 1999. *Daphniphyllum himalaense* subsp. *macropodum* Daphniphyllaceae. *Curtis's Botanical Magazine* **16**: 267–272.
- Cao M, Zhang Y, He H, Li S, Huang S, Chen D, Tang G, Li S, Di Y, Hao X. 2012. Daphniphyllones A–J, alkaloids from *Daphniphyllum macropodum*. *Journal of Natural Products* **75**: 1076–1082.
- Cao MM, Wang L, Zhang Y, He HP, Gu YC, Zhang Q, Li Y, Yuan CM, Li SL, Di YT *et al.* 2013. Daphniphyllones K–O, alkaloids from *Daphniphyllum macropodum*. *Fitoterapia* **89**: 205–209.
- Chattopadhyay AK, Hanessian S. 2017. Recent progress in the chemistry of *Daphniphyllum* alkaloids. *Chemical Reviews* **117**: 4104–4146.
- Cherney EC, Baran PS. 2011. Terpenoid-alkaloids: their biosynthetic twist of fate and total synthesis. *Israel Journal of Chemistry* **51**: 391–405.
- Chowański S, Adamski Z, Marciniak P, Rosiński G, Büyükgüzel E, Büyükgüzel K, Falabella P, Scrano L, Ventrella E, Lelario F *et al.* 2016. A review of bioinsecticidal activity of Solanaceae alkaloids. *Toxins* **8**: 1–28.
- Dong Y, Li B, Aharoni A. 2016. More than pictures: when MS imaging meets histology. *Trends in Plant Science* **21**: 686–698.
- Dong Y, Sonawane P, Cohen H, Polturak G, Feldberg L, Avivi SH, Rogachev I, Aharoni A. 2020. High mass resolution, spatial metabolite mapping enhances the current plant gene and pathway discovery toolbox. *New Phytologist* **228**: 1986–2002.
- Ehmke A, von Borstel K, Hartmann T. 1988. Alkaloid N-oxides as transport and vacuolar storage compounds of pyrrolizidine alkaloids in *Senecio vulgaris* L. *Planta* **176**: 83–90.
- Erb M, Kliebenstein DJ. 2020. Plant secondary metabolites as defenses, regulators, and primary metabolites: the blurred functional trichotomy1. *Plant Physiology* **184**: 39–52.
- Guo L-D, Chen Y, Xu J. 2020a. Total synthesis of *Daphniphyllum* alkaloids: from bicycles to diversified caged structures. *Accounts of Chemical Research* **53**: 2726–2737.
- Guo LD, Hou J, Tu W, Zhang YY, Zhang YY, Chen L, Xu J. 2019. Total synthesis of Dapholdhamine B and Dapholdhamine B lactone. *Journal of the American Chemical Society* **141**: 11713–11720.
- Guo LD, Zhang Y, Hu J, Ning C, Fu H, Chen Y, Xu J. 2020b. Asymmetric total synthesis of yuzurimine-type *Daphniphyllum* alkaloid (+)-caldaphnidine. *Nature Communications* **11**: 3538.
- He T, Zhou Y, Wang YH, Mu SZ, Hao XJ. 2011. Two new alkaloids from *Daphniphyllum angustifolium* hutch. *Helvetica Chimica Acta* **94**: 1019–1023.

- Heathcock CH. 1996. Nature knows best: an amazing reaction cascade is uncovered by design and discovery. *Proceedings of the National Academy of Sciences of the United States of America* 93: 14323–14327.
- Heathcock CH, Davidsen SK, Mills S. 1986. Total synthesis of *Daphniphyllum* alkaloids: (+)-daphnongamine E, (+)-calyciphylline R, and (–)-10-deoxydaphniphylline A. *Journal of the American Chemical Society* 108: 5650–5651.
- Heathcock CH, Joe D. 1995. Possibly biomimetic transformation of the secodaphnane. *The Journal of Organic Chemistry* 60: 1131–1142.
- Heathcock CH, Stafford JA. 1992. *Daphniphyllum* alkaloids. 13. asymmetric total synthesis of (–)-secodaphniphylline. *The Journal of Organic Chemistry* 57: 2566–2574.
- Itkin M, Heinig U, Tzfadia O, Bhide AJ, Shinde B, Cardenas PD, Bocobza SE, Unger T, Malitsky S, Finkers R *et al.* 2013. Biosynthesis of antinutritional alkaloids in solanaceous crops is mediated by clustered genes. *Science* 341: 175–179.
- Kobayashi J, Kubota T. 2009. The *Daphniphyllum* alkaloids. *Natural Product Reports* 26: 936–962.
- Kuhl C, Tautenhahn R, Böttcher C, Larson TR, Neumann S. 2012. CAMERA: an integrated strategy for compound spectra extraction and annotation of liquid chromatography/mass spectrometry data sets. *Analytical Chemistry* 84: 283–289.
- Lee MJ, Pate JS, Harris DJ, Atkins CA. 2007. Synthesis, transport and accumulation of quinolizidine alkaloids in *Lupinus albus* L. and *L. angustifolius* L. *Journal of Experimental Botany* 58: 935–946.
- Li C, Wood JC, Vu AH, Hamilton JP, Rodriguez Lopez CE, Payne RME, Serna Guerrero DA, Gase K, Yamamoto K, Vaillancourt B *et al.* 2023. Single-cell multi-omics in the medicinal plant *Catharanthus roseus*. *Nature Chemical Biology* 19: 1031–1041.
- Li ZY, Gu YC, Irwin D, Sheridan J, Clough J, Chen P, Peng SY, Yang YM, Guo YW. 2009. Further *Daphniphyllum* alkaloids with insecticidal activity from the bark of *Daphniphyllum macropodum* Miq. *Chemistry and Biodiversity* 6: 1744–1750.
- Lichman BR. 2021. The scaffold-forming steps of plant alkaloid biosynthesis. *Natural Product Reports* 38: 103–129.
- Mahroug S, Burlat V, St-Pierre B. 2007. Cellular and sub-cellular organisation of the monoterpenoid indole alkaloid pathway in *Catharanthus roseus*. *Phytochemistry Reviews* 6: 363–381.
- McInnes L, Healy J, Saul N, Großberger L. 2018. UMAP: uniform manifold approximation and projection. *Journal of Open Source Software* 3: 861.
- Minh BQ, Schmidt HA, Chernomor O, Schrempf D, Woodhams MD, Von Haeseler A, Lanfear R, Teeling E. 2020. IQ-TREE 2: new models and efficient methods for phylogenetic inference in the genomic era. *Molecular Biology and Evolution* 37: 1530–1534.
- Mithöfer A, Boland W. 2012. Plant defense against herbivores: chemical aspects. *Annual Review of Plant Biology* 63: 431–450.
- Morehouse NJ, Clark TN, McMann EJ, van Santen JA, Haeckl FPJ, Gray CA, Lington RG. 2023. Annotation of natural product compound families using molecular networking topology and structural similarity fingerprinting. *Nature Communications* 14: 308.
- Morita H, Kobayashi J. 2007. *Daphniphyllum* alkaloids: structures, biogenesis, and activities. In: Fattorusso E, Tagliatela-Scafati O, eds. *Modern alkaloids: structure, isolation, synthesis and biology*. Weinheim, Germany: Wiley-VCH, 541–589.
- Mu SZ, Wang JS, Yang XS, He HP, Li CS, Di YT, Wang Y, Zhang Y, Fang X, Huang LJ *et al.* 2008. Alkaloids from *Daphniphyllum oldhami*. *Journal of Natural Products* 71: 564–569.
- Niwa H, Hirata Y, Suzuki KT, Yamamura S. 1973. Biosynthesis of daphnilactone-B. *Tetrahedron Letters* 14: 2129–2132.
- Niwa H, Toda M, Ishimaru S, Hirata Y, Yamamura S. 1974. Chemical studies on nitrogen heterocyclic skeleton of the *Daphniphyllum* alkaloids. *Tetrahedron* 30: 3031–3036.
- Nothias LF, Petras D, Schmid R, Dührkop K, Rainer J, Sarvepalli A, Protzyuk I, Ernst M, Tsugawa H, Fleischauer M *et al.* 2020. Feature-based molecular networking in the GNPS analysis environment. *Nature Methods* 17: 905–908.
- Pietre S, Heathcock CH. 1990. Biomimetic total synthesis of proto-daphniphylline. *Science* 248: 1532–1534.
- Pluskal T, Weng JK. 2018. Natural product modulators of human sensations and mood: molecular mechanisms and therapeutic potential. *Chemical Society Reviews* 47: 1592–1637.
- Saito S, Yahata H, Kubota T, Obara Y, Nakahata N. 2008. Calyciphyllines H–M, new *Daphniphyllum* alkaloids from *Daphniphyllum calycinum*. *Tetrahedron* 64: 1901–1908.
- Shuzhen M, Chengjian T, Xiaojiang H. 2013. Regional difference of alkaloids from two kinds of medical plant *Daphniphyllum Oldhami* distributed in Guizhou province. *Guangdong Chemical Industry* 40: 31–32.
- Sorokina M, Merseburger P, Rajan K, Yirik MA, Steinbeck C. 2021. Coconut online: collection of open natural products database. *Journal of Cheminformatics* 13: 1–13.
- Suzuki KT, Okuda S, Niwa H, Toda M, Hirata Y, Yamamura S. 1973. Biosynthesis of *Daphniphyllum* alkaloids. *Tetrahedron Letters* 11: 799–802.
- Veselkov K, Sleeman J, Claude E, Vissers JPC, Galea D, Mroz A, Laponogov I, Towers M, Tonge R, Mirnezami R *et al.* 2018. BASIS: High-performance bioinformatics platform for processing of large-scale mass spectrometry imaging data in chemically augmented histology. *Scientific Reports* 8: 4053.
- Wang M, Carver JJ, Phelan VV, Sanchez LM, Garg N, Peng Y, Nguyen DD, Watrous J, Kapon CA, Luzzatto-Knaan T *et al.* 2016. Sharing and community curation of mass spectrometry data with global natural products social molecular networking. *Nature Biotechnology* 34: 828–837.
- Weiss ME, Carreira EM. 2011. Total synthesis of (+)-daphmanidin E. *Angewandte Chemie* 50: 11501–11505.
- Wink M. 1986. Storage of quinolizidine alkaloids in epidermal tissues. *Zeitschrift für Naturforschung - Section C Journal of Biosciences* 41c: 375–380.
- Wink M. 2015. Modes of action of herbal medicines and plant secondary metabolites. *Medicine* 2: 251–286.
- Witte L, Ehmke A, Hartmann T. 1990. Interspecific flow of pyrrolizidine alkaloids. *Naturwissenschaften* 77: 540–543.
- Wu H, Zhang X, Ding L, Chen S, Yang J, Xu X. 2013. *Daphniphyllum* alkaloids: recent findings on chemistry and pharmacology. *Planta Medica* 79: 1589–1598.
- Xiang R, Wang W, Yang L, Wang S, Xu C, Chen X. 2021. A comparison for dimensionality reduction methods of single-cell RNA-seq data. *Frontiers in Genetics* 12: 646936.
- Yamamoto K, Takahashi K, Caputi L, Mizuno H, Rodriguez-Lopez CE, Iwasaki T, Ishizaki K, Fukaki H, Ohnishi M, Yamazaki M *et al.* 2019. The complexity of intercellular localization of alkaloids revealed by single cell metabolomics. *New Phytologist* 224: 848–859.
- Yamamoto K, Takahashi K, Mizuno H, Anegawa A, Ishizaki K, Fukaki H, Ohnishi M, Yamazaki M, Masujima T, Mimura T. 2016. Cell-specific localization of alkaloids in *Catharanthus roseus* stem tissue measured with Imaging MS and Single-cell MS. *Proceedings of the National Academy of Sciences, USA* 113: 3891–3896.
- Yang J, Liu X, Fu J, Lyu HY, Bai LP, Jiang ZH, Zhu GY. 2021. Calycindaphines A–J, *Daphniphyllum* alkaloids from the roots of *Daphniphyllum calycinum*. *RSC Advances* 11: 9057–9066.
- Zhang CR, Liu HB, Dong SH, Wu Y, Yue JM. 2013. Alkaloids from the twigs and leaves of *Daphniphyllum macropodum*. *Helvetica Chimica Acta* 96: 499–504.
- Zhang CR, Liu HB, Feng T, Zhu JY, Geng MY, Yue JM. 2009. Alkaloids from the leaves of *Daphniphyllum subverticillatum*. *Journal of Natural Products* 72: 1669–1672.

## Supporting Information

Additional Supporting Information may be found online in the Supporting Information section at the end of the article.

**Fig. S1** *Daphniphyllum* alkaloid compound subtypes.

**Fig. S2** Feature-based molecular network.

**Fig. S3** Alkaloid subtype annotations in molecular clusters.

**Fig. S4** Comparison of alkaloid annotation methods.

**Fig. S5** Dimensionality reduction and guided clustering approach.

**Fig. S6** Molecular cluster distribution across *Daphniphyllum macropodum* plants.

**Fig. S7** Genotypes of *Daphniphyllum macropodum* accessions.

**Fig. S8** Distribution of alkaloids across *Daphniphyllum macropodum* tissues.

**Fig. S9** Inter-tissue *Daphniphyllum macropodum* metabolomics analysis.

**Fig. S10** Alkaloid subtype enrichment across *Daphniphyllum macropodum* tissues.

**Fig. S11** Tissue distribution of specific peaks across multiple *Daphniphyllum macropodum* plants.

**Fig. S12** Ion intensity maps of selected alkaloids in *Daphniphyllum macropodum* imaging-MS.

**Fig. S13** Imaging-MS of *Daphniphyllum macropodum* young root tissue.

**Fig. S14** Spatial correlations of selected *Daphniphyllum* alkaloids within *Daphniphyllum macropodum* tissues.

**Methods S1** Purification of standards, LC-MS/MS, feature selection and processing, molecular networking and MALDI-MS analysis.

**Table S1** Chemical standards and MS<sup>2</sup> matches.

**Table S2** Untargeted metabolomics samples used in this study of *Daphniphyllum macropodum* alkaloids.

**Table S3** *Daphniphyllum macropodum* individuals used in this study.

**Table S4** *Daphniphyllum* metabolite database.

**Table S5** Sequences used for genotyping *Daphniphyllum macropodum* accessions.

**Table S6** Subtype enrichment across *Daphniphyllum macropodum* tissues.

**Table S7** Alkaloids in *Daphniphyllum macropodum* mass spectral images.

Please note: Wiley is not responsible for the content or functionality of any Supporting Information supplied by the authors. Any queries (other than missing material) should be directed to the *New Phytologist* Central Office.